Chapter 6

Phases of passive colloids in activity driven bath

6.1 Introduction

In the previous chapter.5, we study the properties of polar self-propelled particles along a thin junction. Inside the junction, particles experience a high noise disorder state, and outside they are in the ordered state. The model is motivated by the Josephson junction, an analogous equilibrium system. At the junction, we have found the current orientation reversal for a critical width of the junction, which is a common feature of the Josephson junction. Further, the particle current at the junction decreases with an increase in the junction width Systems with self-propelled or active particles are intrinsically nonequilibrium because each agent consumes energy in order to move or to exert mechanical forces [Bechinger et al. (2016); Li et al. (2019); Marchetti et al. (2013b); Palacci et al. (2013); Rigato et al. (2017)]. Interestingly, these systems show various phenomena like, long ranged ordering in two-dimensions, giant density fluctuations, non-equilibrium order-disorder phase transition, phase separation, etc. In broad self-propelled particles can be classified into two types: particles with asymmetric shape, which have tendency to align along their long

axis, for example, bird, fish, elongated rods, etc. Also, the particles, which are nearly spherical in shape, includes many artificially designed spherical Janus particles in the laboratory. The second class of particles do not have tendency to align, but they move along their direction of polarity. Symmetric self propelled particles, which can move along their direction of asymmetry, but do not have any preferred direction of alignment, are called active Brownian particles (ABPs). Recent study of Fily *et al.* [Solon et al. (2015a)], finds that collection of ABPs can phase separate at a packing density much lower than the corresponding phase separation density in an analogous equilibrium system. The activity or motile nature of the ABPs help them to phase separate at much lower density [Fily & Marchetti (2012)]. Hence the phenomenon is named as motiltiy induced phase separation (MIPS) [Buttinoni et al. (2013); Cates & Tailleur (2015); van Damme et al. (2019)].

Recent studies [Dolai et al. (2018); Liu et al. (2020)], also show an effective attraction between passive Brownian particles or colloids when placed in the medium of ABPs. The phenomena can lead to depletion induced phase separation as found in asymmetric binary mixture of colloids in equilibrium [Asakura & Oosawa (1954); Gratale et al. (2016); Koenderink et al. (1999); Meng et al. (2010); Stradner et al. (2004)]. Surprisingly the depletion induced attraction in asymmetric equilibrium binary mixture, which is a purely entropy driven phenomena has been found in the mixture of athermal ABPs and passive colloids [Dolai et al. (2018)].

In recent years, the dynamics of large passive colloids in a bath of small ABPs is receiving a lot of attention and it is an area of current interest to the physicists in the context of nonequilibrium statistical mechanics [Chakraborty & Das (2020); Das et al. (2014); Dolai et al. (2018)]. A recent study by Leonardo *et al.* [Bechinger et al. (2016)] show that active baths are capable of mediating effective interactions between suspended large colloidal particles [Angelani et al. (2009)]. Nature of the interaction is short-range attractive, which is similar to the depletion forces in the equilibrium colloidal suspensions [Angelani et al.

(2009)]. Furthermore, a paper by Cacciuto *et al.* find that shape of the colloidal particle plays a crucial role defining the range, strength, and sign of the effective interactions [Harder et al. (2014)]. Besides model based studies, recent experimental study finds that passive particles perform super-diffusive dynamics in short times and normal diffusion in long times when suspended in active bath [Wu & Libchaber (2000)]. However, dynamics are similar to Brownian motion but the long-time effective diffusivity of the passive particles shows dependence on their size and concentration of the active particles [Patteson et al. (2016)].

Two phenomena, motility induced phase separation (MIPS) and active depletion force induced phase separation motivate us to study a binary system of large colloidal particles and small ABPs. Although, numerous studies have been done to understand the phenomenological behavior of the ABPs [Marchetti et al. (2013b)], we still lack detailed understanding of how dynamics of non-active or passive bodies is affected when suspended in a collection of ABPs. This is a very important area of colloidal physics where solvent mediated effective interactions play a crucial role in self-assembly of passive collidal particles.

In this chapter, we study the phase behavior of the passive colloidal particles when placed on a two-dimensional substrate in the presence of athermal active particles. All the particles in our system interact through soft-repulsive force. The ABPs are not subjected to random translational noise;, hence they are *athermal* in nature. Although, the phase separation of active-passive mixture has been discussed in many previous studies [Bechinger et al. (2016)], still a full phase diagram of the passive colloidal particles in terms of the defining parameters like size ratio and activity of the depletants (small ABPs) is still lacking. In this chapter, we discussed in detail how the effective interaction among large colloidal particles changes with the size ratio and the activity of the depletants. In other words, we analyze how MIPS phenomenon of the athermal active particles induce effective interaction among

the passive colloids, and their role in phase behaviour of the pure passive system. Furthermore, using both coarse-grained and microscopic simulations, we find four distinct phases based on the spatial distributions of the passive colloids: (i) homogeneous-disordered phase (HDP), (ii) homogeneous crystalline phase (HCP), (iii) disorder-phase separated phase (DPS), and (iv) phase-separated ordered phase (PSP). We draw a phase diagram in the plane defined by the size ratio and the activity of the depletants, where the different phases are characterized by calculating bond-order parameter and cluster size distribution. We further confirmed the four phases using the full microscopic Langevin dynamic simulation of active-passive mixture for the same range of activity and size ratio.

In the rest of the chapter, we discuss the details of the binary model system in section.6.2. Section.6.3.1 discuss the result of effective force between two passive particles in the presence of small ABPs. In section.6.3.2 we show the effect of the effective force on a pure passive system and characteristics of four phases are discussed in detail in section.6.3.3. Finally, we confirmed the four phases using full microscopic study of binary active-passive system and discuss the results in detail in section.6.5.

6.2 Model

Our system consists of a binary mixture of N_1 small active Brownian particles (ABPs) of radius r_a, and N_2 passive particles of radius r_p moving on a two-dimensional substrate of dimension $L_x \times L_y$. We define size-ratio of the particles $S = r_p/r_a$. Let us represent the position vector of the center of the i^{th} ABP and i^{th} passive particle by $\mathbf{r}_i^a(t)$ and $\mathbf{r}_i^p(t)$, respectively at time t. The orientation of i^{th} ABP is represented by a unit vector $\mathbf{n}_i = (\cos\theta_i, \sin\theta_i)$. The dynamics of the active particle is governed by the overdamped Langevin equation

$$\partial_t \mathbf{r}_i^a = v\mathbf{n_i} + \mu_1 \sum_{j\neq i} \mathbf{F}_{ij} \tag{6.1}$$

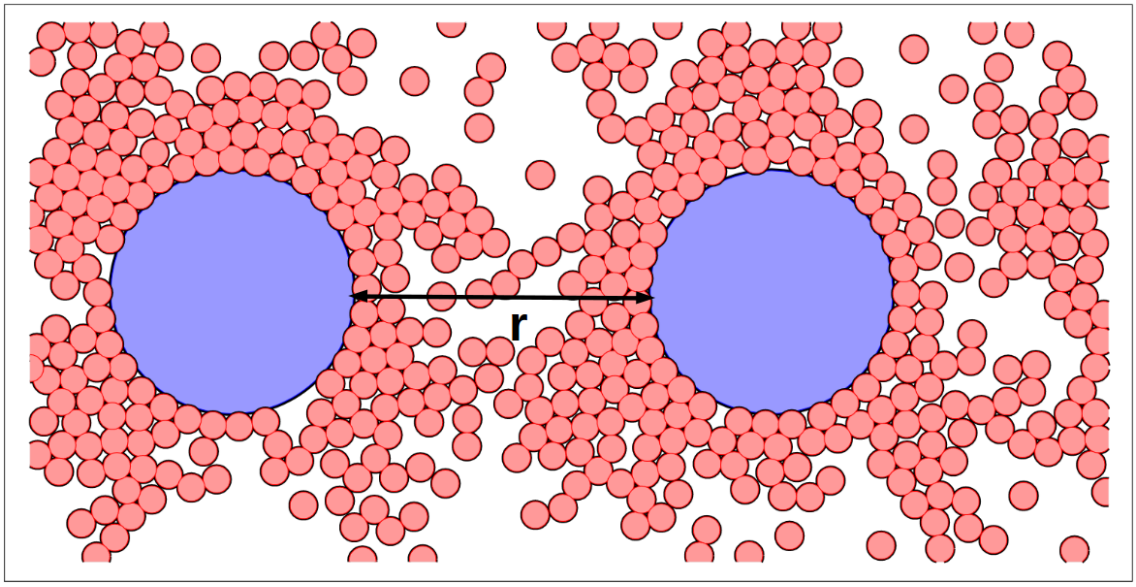

Fig. 6.1 (color online) Plot shows the model picture of small and big ABPs and passive system of $S = 10$ to calculate the effective potential $V^{S,\bar{v}}(r)$ on passive particle separated by distance 'r', exerted by the active depletant. Red particles show the ABPs. Blue and red particles show passive particles and ABPs. The blue arrow line show the surface to surface distance 'r' between two passive particles. Number of ABPs and passive particles are $N_1 = 1000$ and $N_2 = 2$

$$\partial_t \theta_i = \eta_i^r(t) \tag{6.2}$$

$$\partial_t \mathbf{r}_i^p = \mu_2 \sum_{j \neq i} \mathbf{F}_{ij} \tag{6.3}$$

The first term on the right hand side (RHS) of Eq $\sim$ 6.1 is due to the activity of the ABPs with active self-propulsion speed v. The rate of change of the orientation θ_i of the i^{th} ABP is given by Eq $\sim$6.2. The stochastic force $\eta_i^r(t)$ at time t is defined as, $\langle \eta_i^r(t)\eta_j^r(t^{'})\rangle = 2\nu_r\delta_{ij}\delta(t-t^{'})$. ν_r represents the rotational diffusion constant. The persistent length of the ABPs is defined as $l = v/\nu_r$, and the corresponding persistent time $\tau = 1/\nu_r$. We define the dimensionless activity $\bar{v} = \frac{v}{r_a \nu_r}$. The rotational diffusion constant is kept fixed at $\nu_r = 0.005$. The size of the active particles $r_a = 0.1$, The equation of motion

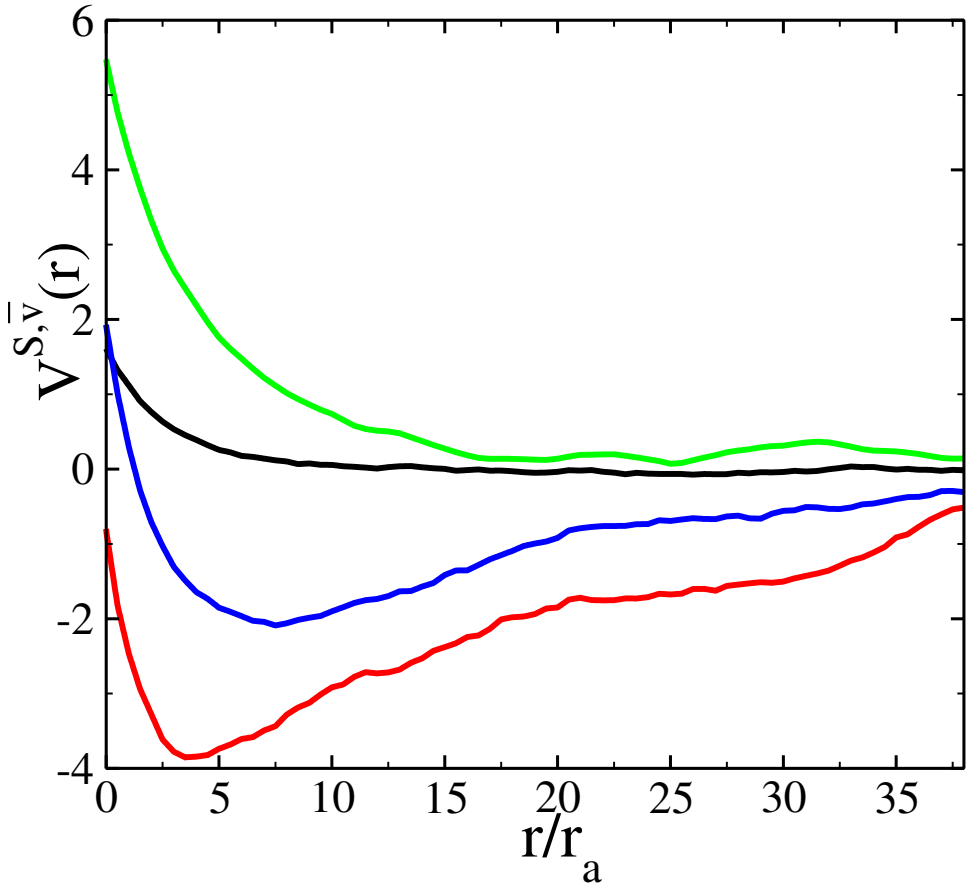

Fig. 6.2 (color online) Plot shows the potential $V^{S,\bar{v}}$ on passive particles in the presence of active depletant for different parameters $(S,\bar{v})$. Black curve $(5,60)$, green curve$(10,40)$, blue curve $(5,160)$ and red curve $(10,160)$ respectively. In all cases number of passive particles $N_2 = 2$ and active particles are $N_1 = 1000$.

to update the position of passive particle is given in Eq ∼6.3 . The force term $\mathbf{F}_{ij}$ in both equations is due to soft repulsive steric interaction between the particles. The force is effective when particles start to touch each other and zero otherwise. The force is obtained from the soft-repulsive pair potential $\mathbf{F}_{ij} = -\nabla U(r_{ij})$, where $U(r_{ij}) = k(r_{ij} - (r_{\beta i} + r_{\beta' j}))^2$ if $r_{ij} \leq (r_{\beta i} + r_{\beta' j})$ and r_β, is the radius of active or passive particles for β and $\beta' = a$ or p respectively. The mobility of both types of particles are kept the same $\mu_1 = \mu_2 = 1.0$ and the force constant $k = 1.0$; hence $(\mu_1 k)^{-1} = 1.0$ defines the elastic time scale in the system. The volume fraction of the ABPs is $\phi_a = N_1 \pi r_a^2/(L_x \times L_y)$. The volume fraction of ABPs is kept fixed at $\phi_a = 0.49$, whereas volume fraction of passive particles depends

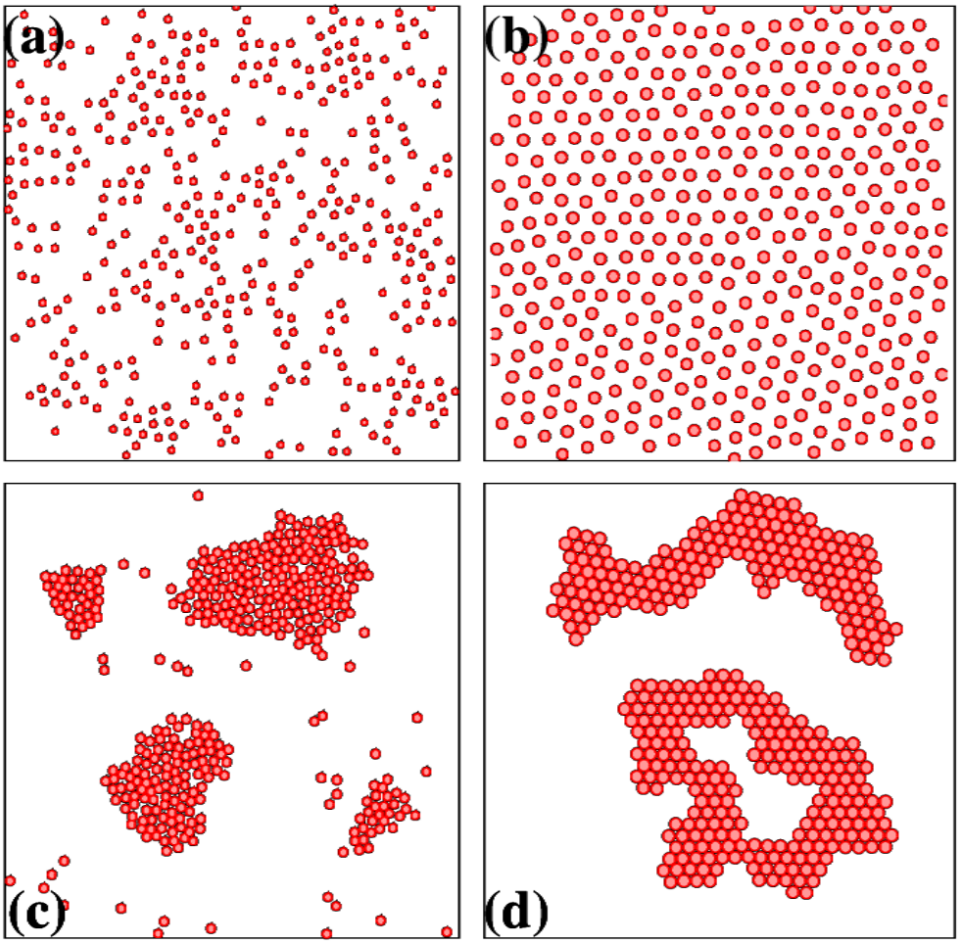

Fig. 6.3 (color online) Steady-state snapshots for four phases of the passive particles interacting through the potential obtained with different combinations of activity $\bar{v}$ and size ratio S. (a) HDP, for $S, \bar{v} = 5, 60$ and packing fraction $\phi_p = 0.07$. (b) HCP for $S, \bar{v} = 10, 40$ for $\phi_p = 0.2$. (c) DPS , for $S, \bar{v} = 5, 160$ for $\phi_p = 0.07$. (d) OPS for $S, \bar{v} = 10, 160$ and packing fraction $\phi_p = 0.2$. In all cases total number of passive particles are $N_2 = 400$

on the size of passive particles. Periodic boundary condition is used in both directions. The smallest time step considered is $\Delta t = 0.001$. One simulation step is counted after the update of all the particles once. Total simulation time is used 10^6 time steps. The size ratio S and dimensionless activity $(S, \bar{v})$ are two control parameters and they are varied from (1 to 10), and (20 to 160).

6.3 Results

6.3.1 Calculation of depletion force

We first calculate the force between two bigger passive particles in the presence of active depletant. To calculate this we place two passive particles of radius r_a in the sea of ABPs. System is evolved to reach to the steady state. The effective potential and force between passive particles are calculated for different radial distances (separation) between them. The model picture of the part of the system at a fixed separation distance of passive particles is shown in Fig.6.1. While doing so, we fix the position of passive colloids to a fixed distance, and active particles are evolving according to the Eqs $\sim$ 6.1 and 6.2. Once steady state configuration of system is achieved, then we move the passive particles to the new position and the same has been repeated. This procedures is repeated starting from overlapping passive particles to the distance between passive particles $12r_a$. Once steady state is reached then with the help of final configuration the force $\mathscr{F}^{S,\bar{v}}(r)$ between two-passive particles and then the potential is calculated by integrating the force over the distance $V^{S,\bar{v}}(r) = \int \mathscr{F}^{S,\bar{v}}(r)dr$. To improve the quality of data, many independent realisations (200) of the similar sytem is designed

The result of the effective potential between two passive particles $V^{S,\bar{v}}(r)$ is shown in Fig.6.2 for different size ratio S and activity $\bar{v}$. We found that potential between two passive particles very much depends on the system parameters. It can be tuned from weakly interacting $(S,\bar{v}) = (3,160)$. Mainly repulsion $(S,\bar{v}) = (10,40)$. Small distance repulsion to moderate distance attraction for $(S,\bar{v}) = (7,160)$ and finally, only large attraction for $(S,\bar{v}) = (10,160)$ shown in Fig.6.2 . In Fig.6.2 the potential is plotted as a function of surface to surface scaled r/r_a distance between passive particles for the four different types as discussed above. For all the cases, potential approaches to zero or particles become non-interacting after the distance $r \geq 40r_a$.

6.3.2 Coarse-grained simulation of pure passive system

Now, we understand the effect of the effective potential calculated for different size ratios and activity on the pure passive system. We start with $N_2 = 400$ number of passive particles on a two-dimensional substrate with $800r_a \times 800r_a$ under the effect of potential obtained in previous section. The position update of passive particles is given by overdamped Langevin equation

$$\partial_t \mathbf{r}_i^p = \mu_2 \sum_{j \neq i} \mathscr{F}_{ij}^{S,\bar{v}} + \sqrt{2D_T}\eta_i^R(t). \tag{6.4}$$

The first term on the right-hand-side (RHS) of Eq ∼6.3 defines the interaction force $\mathscr{F}_{ij}^{S,\bar{v}}$ between the passive particles pair i and j. The force is given by $\mathscr{F}_{ij}^{S,\bar{v}} = -\nabla V_{ij}^{S,\bar{v}}(r)$, where r is the separation between i^{th} and j^{th} passive particle and $V^{S,\bar{v}}$ is the depletion potential as defined in the previous section for the size ratio S and activity $\bar{v}$ of the depletant ABPs. The translational noise $\eta_i^R(t)$ at time t is defined as, $\langle \eta_i^R(t)\eta_j^R(t^{'})\rangle = \delta_{ij}\delta(t-t^{'})$. $D_T = 1.0$ represents the translational diffusion constant. All other parameters are same as defined in section 6.2. The size of the passive particles are kept as for the corresponding effective potential. One simulation step is counted after position update of all the passive particles using Eq ∼6.4. We consider total simulation time steps $t = 5 \times 10^6$. All the physical quantities calculated here are averaged over 50 realisations.

6.3.3 Four distinct phases

We explore the coarse-grained simulation of pure passive system with the potential obtained from the previous section 6.3.1. We start with a random position of passive particles, and the particles are updated using Eq ∼6.4 for the corresponding potentials of different parameters. We waited for the system to reach to the steady state. In Figs.6.3(a)-(d), we show the real space snapshots of particles position for different system parameters $(S,\bar{v}) = (5,60)$,$(10,40)$,$(5,160)$ and $(10,160)$ respectively. Clearly, for the four sets of

the parameters, the passive particles show completely different structures. We identify four distinct phases with respect to their size ratio S that characterise the distribution of the passive particles in the mixture. First, (1) *Homogeneous disorder phase* (HDP): $(S,\bar{v}) = (5,60)$: here there is no clustering of passive particles, and they are found to be homogeneously distributed as shown in Fig.6.3(a). (2) *Homogeneous crystalline phase* (HCP): $(S,\bar{v}) = (10,40)$: here, the passive particles do form big interconneted clusters and arranged periodically on the substrate at a larger distance to the radius of passive particles as shown in Fig.6.3(b). (3) *Disorder phase separated* (DPS): $(S,\bar{v}) = (5,160)$: here the passive particles form big clusters, but the particles are distributed homogeneously within the cluster (without any specific structure) shown in Fig.6.3 (c), and finally, (4) *Ordered phase separated* (OPS): $(S,\bar{v}) = (10,160)$: here the particles are arranged in a periodic fashion and formed big cluster shown in Fig.6.3(d). We further characterise the four phases using observables: cluster size distribution (CSD), the mean size of the cluster, bond-order parameter, the scaled separation between particles. The detailed analysis of four phases have been discussed in the phase diagram shown in Fig.6.5. Now, we discuss each the observable to characterise the different phases.

Cluster size distribution (CSD)

A cluster is defined as a set of particles connected by a most probable distance r_0 depending on the size of the particles. A cluster of size n has $n-$particles cluster. We further calculate the fraction of cluster of size n or cluster size distribution $P(n)$. The normalised (CSDs) of passive particles $P(n)$ for different scaled velocities $\bar{v}$ and size ratio S are plotted in Fig.6.4 for four phases shown in Fig.6.3. In Figs.6.4(a) and (b), we show the CSD for homogeneous disordered phase (HDP) as shown in Fig.6.3(a) for S=4 with different $\bar{v} = 60,80,100$ and for fixed $\bar{v} = 60$ for different S=2,3,4 respectively. We observe that in both plots for given set of S and $\bar{v}$, CSD show the small clusters as shown. In Figs.6.4(c) and (d), we plot the

CSD, $P(n)$ for fixed S=10 with varying activity $\bar{v} = 1, 2$ and for fixed $\bar{v} = 40$ with different $S = 8, 9$ and 10 for the homogeneous crystal phase (HCP) 6.3(b). $P(n)$ is non-monotonic for small n and power law decay for large n, hence for small $\bar{v}$ and big S, we find bigger interconnected clusters. In Figs.6.4(e) and (f), we show the CSD for disordered phase separated phase (DPS) keeping fixed S=7 for different $\bar{v} = 120, 140, 160$ and fixed $\bar{v} = 160$ for different S=5,6,7 respectively. $P(n)$ is non-monotonic for small n and power law decay for large n, hence for $\bar{v} > 100$ and moderate S, we find bigger interconnected disorder clusters. Furthermore, in Figs.6.4(g) and (h), we show the CSD for ordered phase separated (OPS) phase as shown in Fig.6.3(d) for S=10 with different $\bar{v} = 120, 140, 160$ and fixed $\bar{v} = 160$ for different S=8,9,10 respectively. $P(n)$ is non-monotonic for small n and power law decay for large n, hence for $\bar{v} \geq 80$ and big $S \geq 8$, we find bigger interconnected ordered clusters.

We also calculate the mean cluster size, bond order parameter and the mean scaled separation between passive particles (defined later). Based on the above four observables, we characterise the four phases as discussed in 6.3.3. We calculate the mean cluster size by defining $m = \int nP_p(n)dn$ as shown in Fig.6.5(b). To calculate the mean scaled separation we first calculate the most probable distance r_0 among the passive nearest neighbour particles. We define the mean scaled separation $\bar{r}^{-1} = \frac{2r_p}{r_0}$. Particles form homogeneous phase if most probale distance $r_o > 2r_p$, and hence scaled separation distance $\bar{r} > 1.0$ however, for the clustered phase $r_0 < 2r_p$ viz; $\bar{r} \leq 1.0$, where $\bar{r}$ is a measure of surface to surface scaled distance between two neighbouring particles.

Hence, if we find $1/\bar{r} \geq 1.0$ it is phase separated phase however if $1/\bar{r} \leq 1.0$ it is homogeneousely placed particles as shown in Fig.6.5(c). Further, To characterise the structural ordering in the system, we calculate the bond order parameter [Eslami et al. (2018)]. Bond order parameters are used to calculate either global or local average structures of specified particles relative to its neighbours. The bond parameter for hexagonal

structure ψ_6 in two-dimensions is defined as:

$$\psi_m = \frac{1}{N_2}\sum_{l=1}^{N}\sqrt{\frac{1}{N_2}\sum_{j=1}^{N} e^{i6\theta_i}} \tag{6.5}$$

such that $0 \leq \psi_6 \leq 1$. For order phase $\psi_6 \geq 0.6$ and it is $\psi_6 \leq 0.5$ for disorder phase as shown in Fig.6.5(a). Now in the next section of result 6.4 we plot the phase diagram in $S - \bar{v}$ plane on the basis of three observables ψ_6, m, and $1/\bar{r}$ results obtain in this section for four different phases.

6.4 Phase diagram

In this section, we discuss the phase diagram for the four phases. We describe in the plane of size ratio and activity $(S, \bar{v})$. In Fig.6.5, we show the color plot of ψ_6, m and $\bar{r}$ in the phase plane. We find that for small $S \leq 4$ for all $\bar{v}$, passive particles are always in homogeneous disorder phase (HDP) with small $\psi_6 \leq 0.2$, $m < 3$ and $\bar{r}^{-1} \leq 1.0$ as shown by the circles in the phase diagram in Figs6.5(a)-(c). For large $S \geq 8$ and small activity $\bar{v} \leq 2$ we find large $\psi_6 \geq 0.6$, large $m \geq 9$ and large $\bar{r}^{-1} \leq 1.0$. This phase we called as homogeneous crystalline phase (HCP) shown by triangle. For $S \leq 7$ and large $\bar{v} \geq 100$, particles do show phase separation, with lesser order hence moderate $0.2 \leq \psi_6 \leq 0.6$, small $m \leq 7$ and $\bar{r}^{-1} \geq 1.0$ shown by pentagon and we call this phase as disordered phase separated (DPS). Further, for large $S \geq 8$ and $\bar{v} \geq 80$, particles are distributed uniformaly on the system with periodic hexagonal structure, hence we find large $\psi_6 > 0.6$, large $m \geq 9$ and $\bar{r}^{-1} \geq 1.0$. This phase is called as ordered phase separated (OPS) phase with square symbol.

6.5 Discussion

We have studied the steady-state feature of binary mixtures of small active and big passive athermal particles on a two dimensional substrate, interacting via soft repulsive force with Langevin's simulation. The size ratio of passive and active particles, and activity of ABPs are tuned by S and $\bar{v}$. The motility of small ABPs induces an effective force between big passive particles and it is very much depends upon the system parameters viz; S and $\bar{v}$. Later on we simulate the pure passive particles in the presence of potential (or force) obtained from the various system parameters. Depending on the potential, we observe four distinct phases. For small size ratio and all activity potential or force acting between passive particles are less interacting; hence we find HDP. Whereas for low activity and big size ratio, potential is mainly repulsive and hence particles show HCP. For moderate size ratio and high activity, force is small distance repulsive and large distance attractive, hence passive systems shows a DPS. Finally, for large activity and size ratio potential is purely attractive particles form OPS. These four phases are further characterised by CSD, mean cluster size, mean separation distance, and finally, the structural arrangement is confirmed by calculating the bond order parameter ψ_6 shown in the phase diagram in S-$\bar{v}$ plane for three observables ψ_6, m and $1/\bar{r}$

At the end we confirmed all the four phases using full microscopic simulation of active-passive mixture as shown in Fig.6.6. The update equations for active-passive are similar to Eqs ∼6.1,6.2 and 6.3. The packing fraction for active and passive particles keeping fixed to $\phi_a = 0.5$ and $\phi_p = 0.2$ respectively. in Fig.6.6(a) represents the HDP for $(S, \bar{v}) = (5, 60)$. in Fig.6.6(b) shows the HCP for $(S, \bar{v}) = (10, 40)$, in Fig.6.6(c) represents DPS for $(S, \bar{v}) = (7, 160)$. Fig.6.6(d) shows the OPS for $(S, \bar{v}) = (10, 160)$.

Our study explores new approach to find the effective potential acted among the passive particles in the presence of activity driven bath and phase behaviour of passive particles.

Our model can be useful to understand the phase behaviour of real colloidal systems in active medium.

****

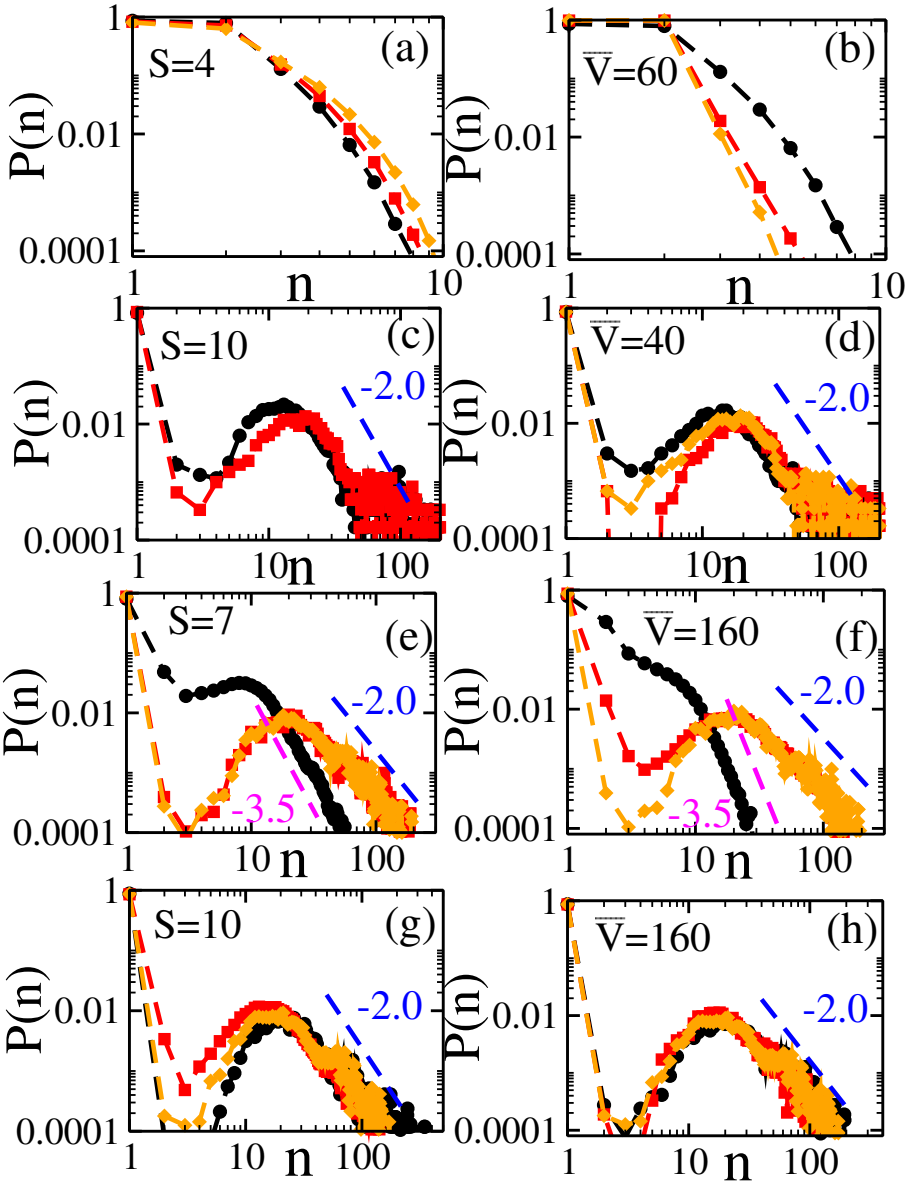

Fig. 6.4 (color online) We plot cluster size distribution CSD, $P(n)$ vs. mean number of particles cluster n for four distinct phases. For HDP: (a) show the CSD for fixed S=4 for different activity $\bar{v} = 60$ (black circles), $\bar{v} = 80$ (red square), $\bar{v} = 100$ (orange diamonds) and (b) is for fixed $\bar{v} = 60$ for different size ratio S=2 (black circle), S=3 (red square) and S=4 (orange diamond). For HCP:(c) show the CSD for fixed S=10 for different activity $\bar{v} = 20$ (black circles) and $\bar{v} = 40$ (red square) and (c) is for fixed $\bar{v} = 40$ for different size ratio S=8 (black circle), S=9 (red square) and S=10 (orange diamond). For DPS:(e) show the CSD for fixed S=7 for different activity $\bar{v} = 120$ (black circles), $\bar{v} = 140$ (red square), $\bar{v} = 160$ (orange diamonds) and (f) is for fixed $\bar{v} = 160$ for different size ratio S=5 (black circle), S=6 (red square) and S=8 (orange diamond). Finally, for OPS:(g) show the CSD for fixed S=10 for different activity $\bar{v} = 120$ (black circles), $\bar{v} = 140$ (red square), $\bar{v} = 160$ (orange diamonds) and (h) is for fixed $\bar{v} = 160$ for different size ratio S=8 (black circle), S=9 (red square) and S=10 (orange diamond). Other details are same as in Fig.6.3. Blue and pink lines show the slope of 2.0 and 3.5 respectively.

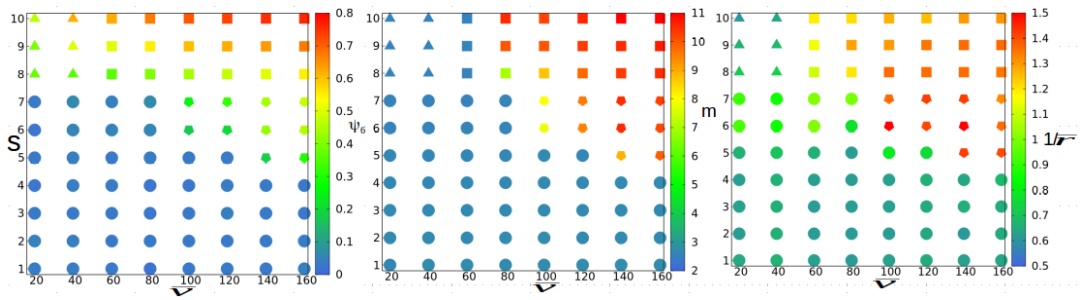

Fig. 6.5 (color online) In this plot (a),(b), and (c), we show the phase diagram in S-$\bar{v}$ plane for ψ_6, mean cluster size m, and mean normalise distance r. In all the plots number of passive particles are 400.

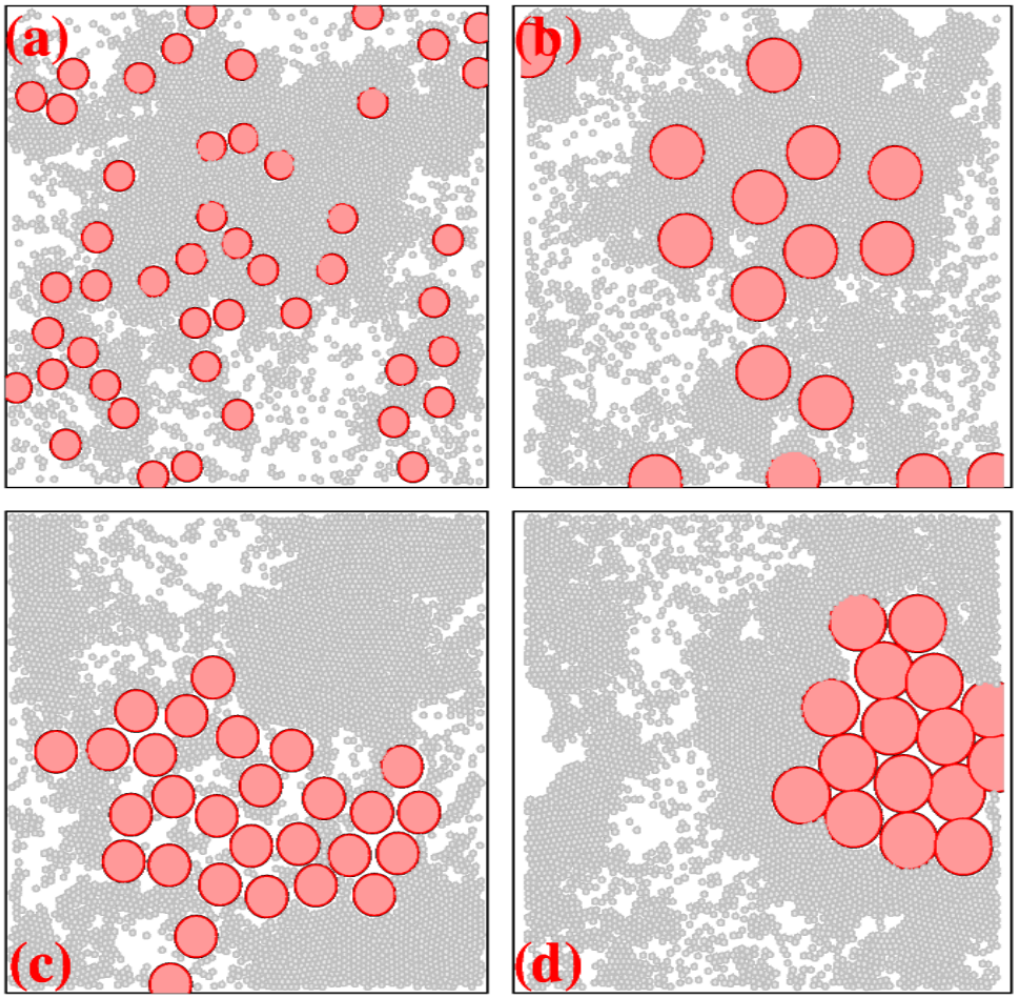

Fig. 6.6 (color online) Plot (a)-(d) show the distinct four phases obtained from microscopic simulation of ABPs and passive mixture with packing fraction $\phi_a = 0.5$ and $\phi_p = 0.2$. (a) represents the HDP for $(S, \bar{v}) = (5, 60)$. (b) shows the HCP for $(S, \bar{v}) = (10, 40)$. (c) represents DPS for $(S, \bar{v}) = (7, 160)$. (d) shows the OPS for $(S, \bar{v}) = (10, 160)$. Smaller black particles are ABPs, and bigger are passive one.